

Gaussian Quadrature and Its Application to Infrared Radiation

J. LI

*Canadian Centre for Climate Modelling and Analysis, Atmospheric Environment Service, University of Victoria,
Victoria, British Columbia, Canada*

(Manuscript received 16 October 1998, in final form 14 May 1999)

ABSTRACT

The Gaussian integration of moments is systematically discussed. It is shown that the well-known diffusivity-factor approximation is equivalent to a one-node Gaussian quadrature. The limit as the moment power approaches infinity in a one-node Gaussian quadrature produces a diffusivity factor of $e^{1/2} = 1.648\ 721\ 3$, which is very close to the value of 1.66 suggested by Elsasser.

The errors due to the diffusivity-factor approximation are analyzed in a one-dimensional radiative transfer model. Generally, the results cannot be improved by using other one-node Gaussian quadrature schemes with different moments. More accurate results can be obtained by using higher-node Gaussian quadratures. It is found that the limit as the moment power approaches infinity always produces the best results. The computational advantage of the diffusivity-factor approximation is kept in the higher-node Gaussian quadratures. It is, therefore, feasible to implement the higher-node Gaussian quadratures in climate models.

1. Introduction

For infrared radiation, scattering by gas is very weak and the infrared scattering process is usually neglected. Without scattering, the absorption and emission are the dominate processes for the infrared radiative transfer. This method of neglecting scattering is consequently called the absorption approximation or the emissivity approximation.

In the absorption approximation, the radiance obtained from the radiative transfer has to be converted to flux by angular integration. However, this integration cannot be done in closed form and an approximation has to be used. Elsasser (1942) proposed the diffusivity-factor (DF) approximation by taking an averaged cosine of the local zenith as $1/1.66$. This DF approximation has been widely adopted in the last half century, since it is commonly believed that the error incurred by using the DF approximation is small. Almost all GCMs that use the absorption approximation method for infrared radiative transfer use the DF approximation. Furthermore, the DF approximation can be used in calculations where scattering is considered. However, since Elsasser (1942) proposed the DF approximation, the choice of 1.66 for the diffusivity factor has remained somewhat

ad hoc. Why should the diffusivity factor be 1.66? What is the mathematical or physical basis for it? In addition, there has been no systematic analysis of the accuracy of the DF approximation. The purpose of this paper is to answer these questions. In the following sections, we will study the mathematical basis for the DF approximation and how the DF relates to the other methods for approximate calculation of integrals. We will then demonstrate the validation of the DF and include an estimate of how large the error could be in calculation of flux transmittance by the DF. Next, we will examine how to extend the DF approximation to the corresponding higher-order approximation. Finally, we will study the errors in fluxes and cooling rates incurred by using the DF and other approximation methods in a radiative transfer model.

2. Gaussian quadrature

If the scattering is neglected, the radiative transfer equation for azimuthally averaged diffuse infrared intensity with wavenumber ν is

$$\mu \frac{dI_\nu(\tau_\nu, \mu)}{d\tau_\nu} = (1 - \omega_\nu)I_\nu(\tau_\nu, \mu) - (1 - \omega_\nu)B_\nu(\theta), \quad (1)$$

where μ is cosine of the local zenith angle, τ_ν is the optical depth, ω_ν is the cloud droplet single scattering albedo, and $B_\nu(\theta)$ is blackbody emission at temperature θ . The upward flux at pressure p is given by

Corresponding author address: Dr. Jiangnan Li, Canadian Centre for Climate Modeling and Analysis, Atmospheric Environment Service, P.O. Box 1700, University of Victoria, Victoria, BC V8P 2Y2, Canada.
E-mail: jiangnan.li@ec.gc.ca

$$F_{\nu}^{\uparrow} = B_{\nu}(\theta_s)T[\tau_{\nu}(p, p_s)] - \int_p^{p_s} B_{\nu}(\theta') \frac{\partial T[\tau_{\nu}(p, p')]}{\partial p'} dp', \quad (2a)$$

and the downward flux at pressure p is

$$F_{\nu}^{\downarrow} = \int_0^p B_{\nu}(\theta') \frac{\partial T[\tau_{\nu}(p, p')]}{\partial p'} dp', \quad (2b)$$

where p_s is the surface pressure, θ_s is the surface temperature, θ' is the temperature at pressure p' , and $T[\tau_{\nu}(p, p')]$ is the flux transmittance defined in terms of the optical depth $\tau_{\nu}(p, p')$ for a slab of atmosphere between p and p' ,

$$T[\tau_{\nu}(p, p')] = 2 \int_0^1 \exp[-\tau_{\text{abs},\nu}(p, p')/\mu] \mu d\mu, \quad (3)$$

where

$$\tau_{\text{abs},\nu}(p, p') = \int_{p'}^p [1 - \omega_{\nu}(p'')] \frac{\partial \tau_{\nu}(p, p'')}{\partial p''} dp'',$$

in a clear-sky $\omega_{\nu}(p) = 0$ and $\tau_{\text{abs},\nu}(p, p') = \tau_{\nu}(p, p')$. The integral in Eq. (3) converts the radiance into the flux. However, this integration cannot be done in closed form, and an approximation has to be considered. Elsasser (1942) proposed the DF approximation by taking

$$T(\tau) = 2 \int_0^1 \exp(-\tau_{\text{abs}}/\mu) \mu d\mu \approx \exp(-\tau_{\text{abs}}/\bar{\mu}_1), \quad (4)$$

where $1/\bar{\mu}_1 = 1.66$ is the so-called diffusivity factor. In Eq. (4), the dependence of τ and τ_{abs} on the p , p' , and ν has been omitted.

The advantage of Eq. (4) is that the flux transmittance follows a simple exponential decay law, in the same manner as the radiance transmittance. The definition of the flux transmittance in terms of an exponential function is efficient for a multilayer calculation. If the flux transmittance for each layer is known, the result for any combined adjacent layers is the multiple of the results for each layer, since for two layers of optical depths τ_i and τ_j ,

$$T(\tau_i + \tau_j) = T(\tau_i)T(\tau_j). \quad (5)$$

In the infrared, each layer of the model contains a heat source. One, therefore, needs to be able to calculate the transmittance between layers that are at varying separation. The simple multiplicative nature of the DF approximation shown in Eq.(5) avoids additional computation of exponentials.

We would like to point out another example of the computational advantage of the flux transmittance of the simple exponential form. In the k-distribution method (Chou and Suarez 1994), the mean flux transmittance can be expressed as

$$T = \int_0^{\infty} \exp(-k\bar{q}/\bar{\mu}_1) f(k) dk, \quad (6)$$

where k is the absorption coefficient, \bar{q} is the absorber amount, and $f(k)$ is the k-distribution function. Written in the discrete form, Eq. (6) is

$$T = \sum_n \exp(-k_n \bar{q}/\bar{\mu}_1) f_n \delta k_n. \quad (7)$$

We can choose $k_n = \eta k_{n-1}$, where η is a positive integer. With this choice, only a single exponential function for k_1 is needed. The other exponential terms can thus be obtained by raising the first exponential to an integer power.

The question remains, however, as to the size of the error of the DF approximation itself and the error induced in the radiative transfer calculation by the DF approximation. Intrinsically, the DF approximation in Eq. (4) is a one-node Gaussian quadrature (1GQ) (appendix A). We can directly apply the Gaussian quadrature of Eq. (A1) to calculate the flux transmittance by the formula for either moment power $l = 0$ or $l = 1$. For $l = 0$ we have

$$2 \int_0^1 \exp(-\tau_{\text{abs}}/\mu) \mu d\mu = 2 \sum_{i=1}^n b_i \bar{\mu}_i \exp(-\tau_{\text{abs}}/\bar{\mu}_i), \quad (8)$$

where n is the node number for Gaussian quadrature, $\bar{\mu}_i$ is the abscissa, and w_i is the weight. In Eq. (8), we take the whole $\exp(-\tau_{\text{abs}}/\mu) \mu$ as the function f in Eq. (A1); therefore, it is the zero-moment Gaussian integral and the result is the μ weighted mean (μ WM). For 1GQ, as only one term exists for a hemisphere, we call it the hemispheric mean (Toon et al. 1989). The values of $\bar{\mu}_i$ and w_i for μ WM as a zero moment ($l = 0$) Gaussian quadrature are shown in Table 1 for node $n = 1, 2, 3$.

Taking now μ as the moment power one in the integral of Eq. (4), from Eq. (A1) the corresponding results are

$$2 \int_0^1 \exp(-\tau_{\text{abs}}/\mu) \mu d\mu = 2 \sum_{i=1}^n b_i \exp(-\tau_{\text{abs}}/\bar{\mu}_i). \quad (9)$$

The values for the abscissa $\bar{\mu}_i$ and the weight w_i for moment power $l = 1$ are also shown in Table 1 for nodes $n = 1, 2, 3$.

Furthermore, a Gaussian quadrature with a higher moment power can be used by making the substitution $\mu = x^{(m+1)/2}$ (see appendix A). Under these conditions, the result for $m = 1$ is the same as that for $l = 1$ in Eq. (9), but the result for $m = 0$ is different from that of μ WM in Eq. (8).

For 1GQ(μ WM), we obtain the diffusivity factor $1/\bar{\mu}_1 = 2$, which is much larger than the value of 1.66 chosen by Elsasser (1942). For 1GQ of different moment power we obtain the diffusivity factor $1/\bar{\mu}_1 = 1.414 21, 1.5, 1.5625, 1.587 96, 1.601 80, 1.610 51$, corresponding to $m = 0, 1, 3, 5, 7, 9$, respectively. The diffusivity factor $1/\bar{\mu}_1$ increases slightly as the moment power m increases. However, they are all smaller than 1.66.

TABLE 1. Abscissa and weight factors for Gaussian integration of moments in Eq. (A4).

n	$m = 0$		$m = 1$		$m = 3$	
	x_i	b_i	x_i	b_i	x_i	b_i
1	0.5000000	1.0000000	0.6666667	0.5000000	0.8000000	0.2500000
2	0.2113249	0.5000000	0.3550510	0.1819586	0.5298579	0.0669052
	0.7886751	0.5000000	0.8449489	0.3180414	0.8987135	0.1830947
3	0.1127017	0.2777778	0.2123405	0.0698270	0.3632646	0.0164791
	0.5000000	0.4444444	0.5905331	0.2292411	0.6988113	0.1045999
	0.8872983	0.2777778	0.9114120	0.2009319	0.9379241	0.1289210
n	$m = 5$		$m = 7$		$m = 9$	
	x_i	b_i	x_i	b_i	x_i	b_i
1	0.8571429	0.1666667	0.8888889	0.1250000	0.9090909	0.1000000
2	0.6307916	0.0383376	0.6962145	0.0262674	0.7419995	0.0197866
	0.9247640	0.1283291	0.9401492	0.0987326	0.9503082	0.0802133
3	0.4679832	0.0072970	0.5438333	0.0042224	0.6010331	0.0028227
	0.7616240	0.0645966	0.8027104	0.0458878	0.8316982	0.0352881
	0.9522110	0.0947731	0.9611486	0.0748898	0.9672687	0.0618893

In Fig. 1 the relative errors of flux transmittance for 1GQ(μ WM) and 1GQ with moment power $m = 0, 1, 3, 5, 7, 9$ are shown (dotted lines), as well as the relative error of the DF approximation (solid line in the right figure in the bottom panels). We define the absolute error as the value obtained from the approximation method minus the value obtained using a rigorous method and the relative error as the absolute error divided by the value from the rigorous method. In addition, the flux transmittance versus τ_{abs} based on a precise integral calculation of Eq. (3) is shown (figure in the top panels).

It is found that for $1/\bar{\mu}_1 = 2$, from 1GQ(μ WM), the flux transmittance is relatively accurate in the region of thin τ_{abs} and the relative error increases rapidly as $\tau_{\text{abs}} > 0.3$. Whereas for $1/\bar{\mu}_1 = 1.5$, from 1GQ($m = 1$), the relative error of flux transmittance becomes larger in the region of thin τ_{abs} compared to that of 1GQ(μ WM), but the relative error does not increase so rapidly with the increase of τ_{abs} . A compromise for the extreme cases is $1/\bar{\mu}_1 = 1.66$, as was chosen by Elsasser (1942).

From Fig. 1, it is found that the relative error in the region of thin τ_{abs} always decreases with an increase in the power of the moment. The flux transmittance converges to a limit very slowly, with increasing moment power m . In appendix A, the limit as $m \rightarrow \infty$ is calculated. We obtain $1/\bar{\mu}_1 = e^{1/2} = 1.648\ 721\ 3$ for $m \rightarrow \infty$. This value is very close to $1/\bar{\mu}_1 = 1.66$. The difference between them is about 0.67%.

Because the flux transmittance decreases exponentially as τ_{abs} increases, the absolute error would be very small for a large τ_{abs} . Therefore, the accuracy in the thin τ_{abs} region is very important. However, for the case of 1GQ(μ WM), the relative error exceeds 10% at $\tau_{\text{abs}} = 0.3$. At that value of τ_{abs} , the flux transmittance is still large. Therefore, the absolute error could be large. Whereas for 1GQ($m \rightarrow \infty$), the relative error is less than 10% for τ_{abs} less than 1. Beyond that value of τ_{abs} the

flux transmittance is about one order lower than the unity. The absolute error is therefore very small. Considering the errors for both thin and thick τ_{abs} , we conclude that $1/\bar{\mu}_1 = e^{1/2}$ is very suitable choice for the flux transmittance.

For more accurate results, the two-node Gaussian quadrature (2GQ) could be used. The 2GQ has the same computational advantage as 1GQ shown in Eq. (5), since for two layers of optical depths τ_i and τ_j ,

$$\begin{aligned}
& \sum_{i=1}^2 w_i \exp[-(\tau_{\text{abs}i} + \tau_{\text{abs}j})/\bar{\mu}_i] \\
&= w_1 T_1(\tau_i + \tau_j) + w_2 T_2(\tau_i + \tau_j) \\
&= w_1 T_1(\tau_i) T_1(\tau_j) + w_2 T_2(\tau_i) T_2(\tau_j). \quad (10)
\end{aligned}$$

Only the exponential functions related to each single layer are required in calculation. If 2GQ is applied to the k distribution in Eq. (7), two exponential functions related to k_1 are needed. The other exponential terms can also be obtained by raising the two exponentials related to k_1 to an integer power. In Fig. 1, the relative errors of 2GQ for different values of moment power and the limit of $m \rightarrow \infty$ are shown (dashed lines). Similar to 1GQ, the relative errors in the region of thin τ_{abs} decrease with the increase of m . The limit of $m \rightarrow \infty$ provides the most accurate results in the thin τ_{abs} region. For 2GQ the errors increase rapidly only in the regions beyond $\tau > 3$. In such regions, the flux transmittance becomes very small, about two orders lower than the unity.

For more accurate results, higher-node Gaussian quadrature methods can be used. Figure 1 shows the results of the three-node Gaussian quadrature (3GQ) (long dashed lines in Fig. 1) for different moments and the limit of $m \rightarrow \infty$. In comparison with 2GQ, the relative errors in 3GQ are reduced for both thin and thick

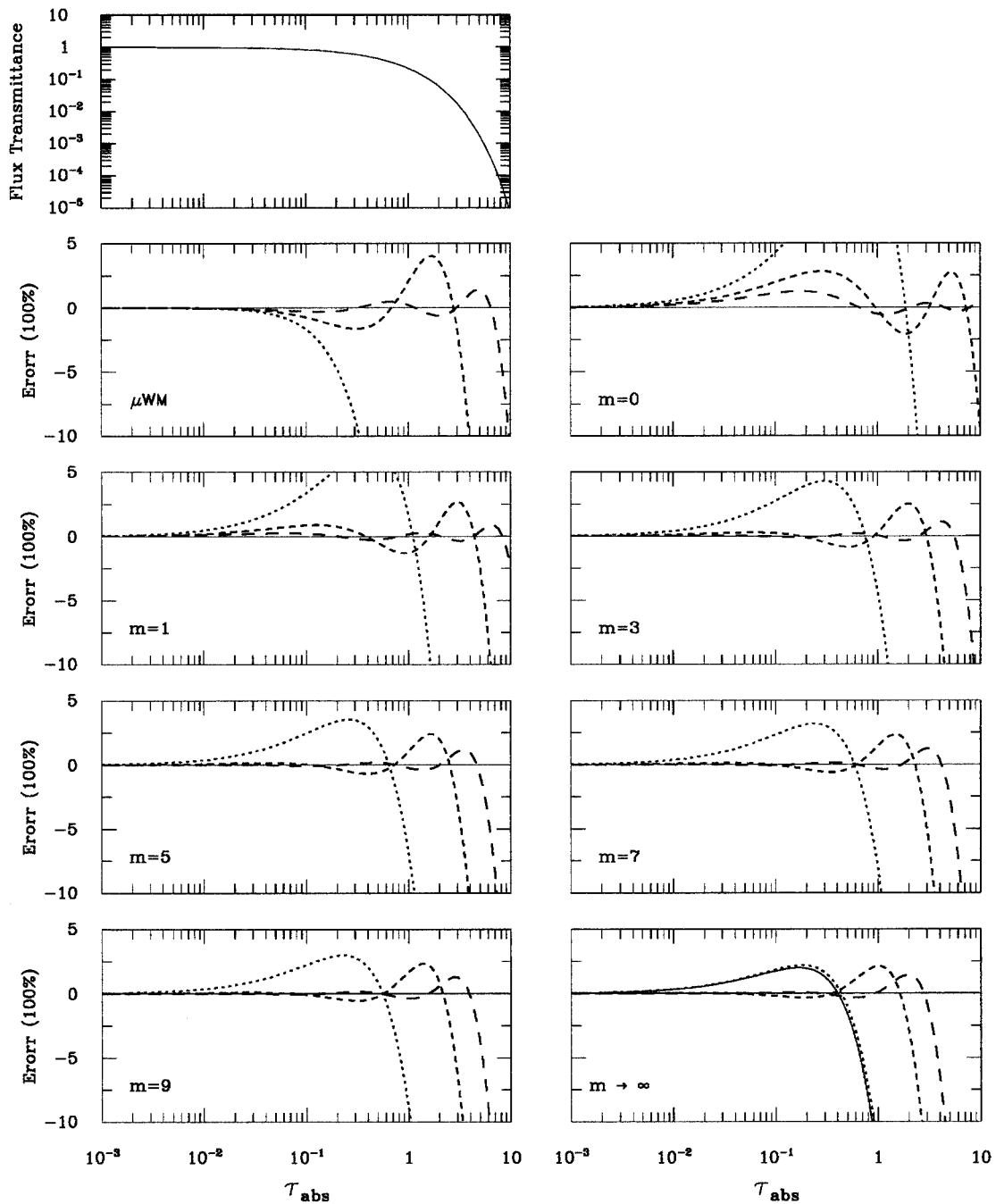


FIG. 1. The figure in the top panels shows the flux transmittance vs τ_{abs} . The rest of the figures show the relative errors of flux transmittance for 1GQ (dotted lines), 2GQ (dashed lines), and 3GQ (long dashed lines). Results for μWM and moment power $m = 0, 1, 3, \dots, 9, \infty$ are shown. The relative error for the DF approximation is shown in the right figure in the bottom panels (solid line).

τ_{abs} . Also, the limit of $m \rightarrow \infty$ provides the most accurate results in the thin τ_{abs} region.

3. Results in one-dimensional model

The infrared radiation model is the same as that of Fu et al.(1997). This model uses the correlated k dis-

tribution with 67 monochromatic calculations for gaseous transmissions and 12 bands for cloud optical properties. The midlatitude summer atmosphere is considered and divided into 100 layers from the surface to 25 km, with a layer thickness of 0.25 km. Benchmark values are obtained from the δ -128-stream discrete ordinate model (Stamnes et al. 1988). The solution of Fu et al.,

Errors in Flux and Cooling Rate

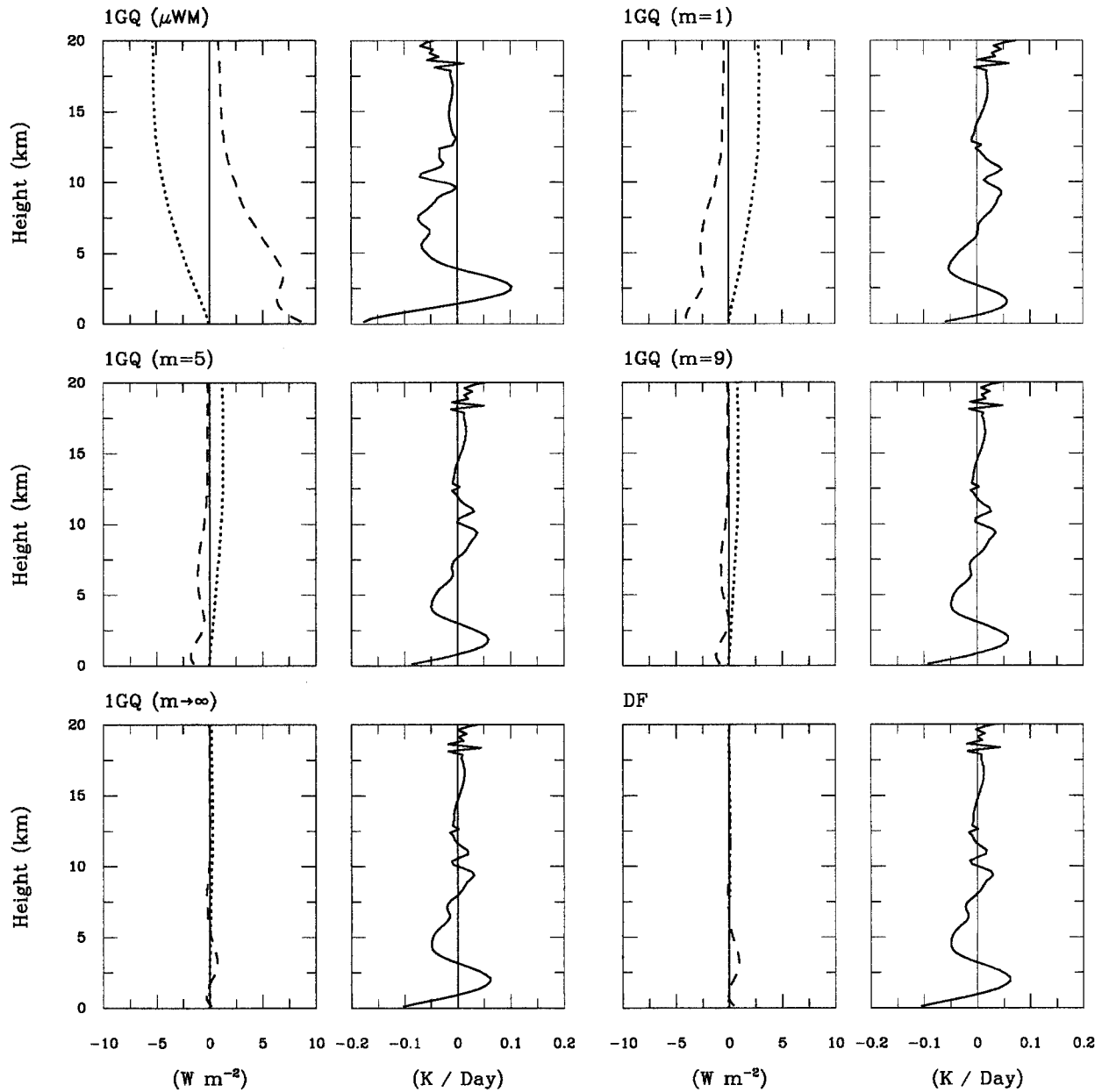


FIG. 2. Absolute errors for upward flux (dotted line), downward flux (dashed line), and cooling rate (solid line) for the DF approximation and 1GQ with different moment powers, m . Midlatitude summer atmosphere with vertical resolution 0.25 km.

(1997) is different from that of Eq. (2). The Gaussian quadrature does not directly apply to flux transmittance in Eq. (4) but applies to the intensity (appendix B).

Figure 2 shows the absolute errors of the DF approximation and 1GQ for the upward flux, downward flux, and cooling rate in the atmosphere. For 1GQ, the cases of μWM and several values of moment power are considered. It is found in Fig. 2 that the absolute error for the DF approximation in the cooling rate is small,

generally less than 0.1 K day^{-1} in the lower atmosphere. The error for the DF approximation in downward flux near the surface is about 0.6 W m^{-2} .

For 1GQ(μWM), the errors for fluxes and cooling rates are much larger than those of the DF approximation, particularly for fluxes. The reason for the poor results of 1GQ(μWM) is that many of the layer gaseous τ_{abs} 's are sufficiently large, so that this method is not accurate. As we mentioned above, 1GQ(μWM) is ac-

Errors in Flux and Cooling Rate

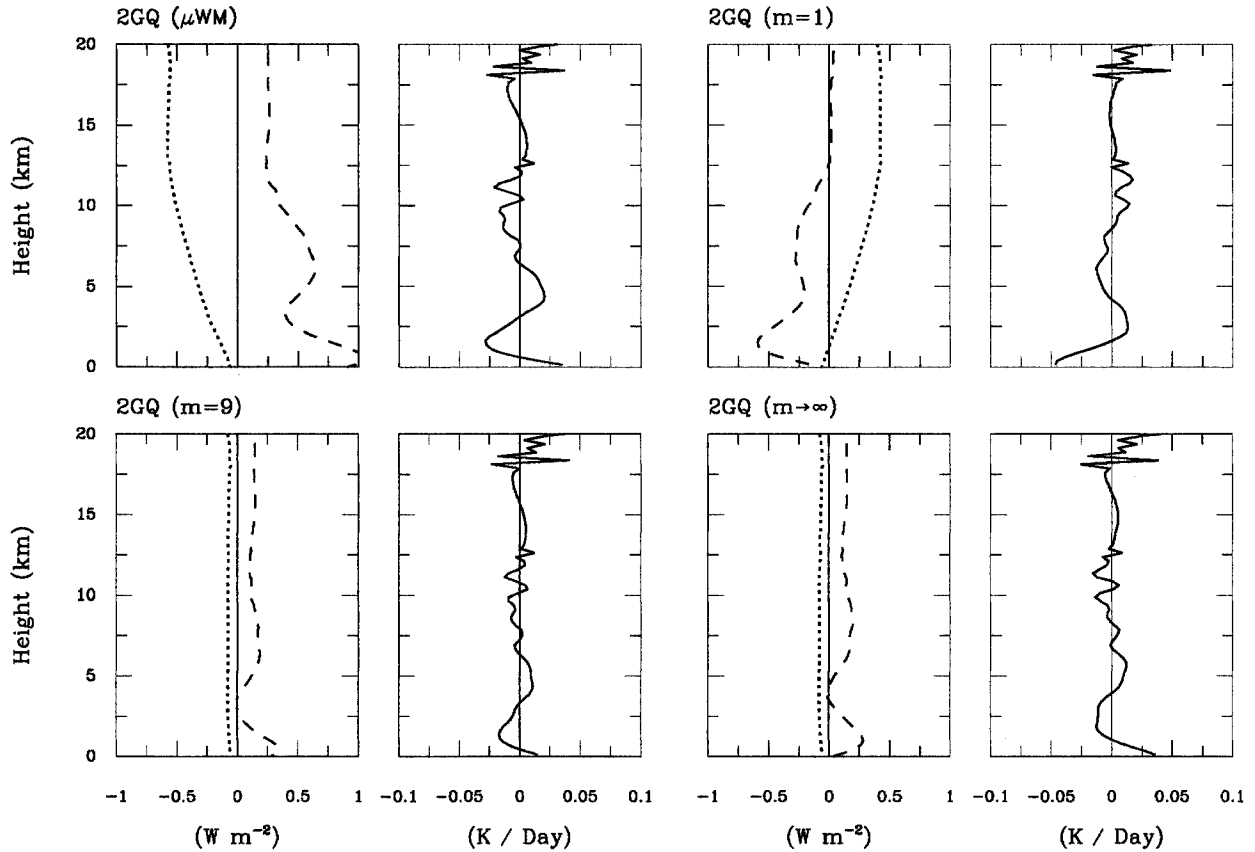


FIG. 3. The same as Fig. 2 but for 2GQ with different moment powers.

curate in flux transmittance for very thin τ_{abs} . The relative error for flux transmission dramatically increases as τ_{abs} exceeds 0.3. For the DF approximation, on the other hand, the calculations are more accurate for larger τ_{abs} 's (see Fig. 1).

Considering 1GQ with different moment powers, we find that the fluxes and cooling rates become more accurate with increasing moment power m . When $m \rightarrow \infty$, the results become very similar to those of the DF approximation. This is expected since the difference in flux transmittance between the DF approximation and 1GQ($m \rightarrow \infty$) is very small, as is shown in Fig. 1.

Figure 3 shows the corresponding results of 2GQ. The physical parameters are the same as those in Fig. 2. It is found that the errors in the cooling rate are generally less than 0.05 K day^{-1} , better than the results in Fig. 2. Like 1GQ the largest errors occur for μWM . It is shown in Fig. 1 that for $\tau_{\text{abs}} < 1$ the error in flux transmittance for 2GQ(μWM) is generally larger than that for 2GQ with moment $m \geq 1$. Also like 1GQ, the errors become smaller with the increase of the moment power m .

Figure 4 shows the corresponding results for 3GQ with the same physical parameters as those in Fig. 3.

In comparison with Fig. 3, the errors are further reduced. The absolute errors in fluxes are less than 1 W m^{-2} for all cases of 3GQ. Like 1GQ and 2GQ, the Gaussian quadratures with moment power $m = 9$ and $m \rightarrow \infty$ produce similar results. In the limit of $m \rightarrow \infty$, the error in flux is less than 0.01 W m^{-2} for the lower atmosphere below 18 km. Since 3GQ($m \rightarrow \infty$) is so accurate, there is no need to consider the four-node Gaussian quadrature.

We now discuss the cloudy-sky case, again using the 100-layer midlatitude summer atmosphere. The same cloud cases as in Fu et al. (1997) are considered. A low cloud is positioned from 1.0 to 2.0 km with a liquid water content (LWC) of 0.22 g m^{-3} and effective radius (r_e) of $5.98 \mu\text{m}$. A middle cloud is positioned from 4.0 to 5.0 km with $\text{LWC} = 0.28 \text{ g m}^{-3}$ and $r_e = 6.2 \mu\text{m}$. A high cloud is positioned from 10 to 12 km, with an ice water content (IWC) of 0.0048 g m^{-3} and mean effective size (D_e) of $41.5 \mu\text{m}$. In the benchmark calculations the cloud infrared scattering is considered but the scattering process is neglected in the absorption approximation, since the purpose of this paper is to show the results of the different Gaussian quadratures on the fluxes and cooling rates; besides, most of GCMs still

Errors in Flux and Cooling Rate

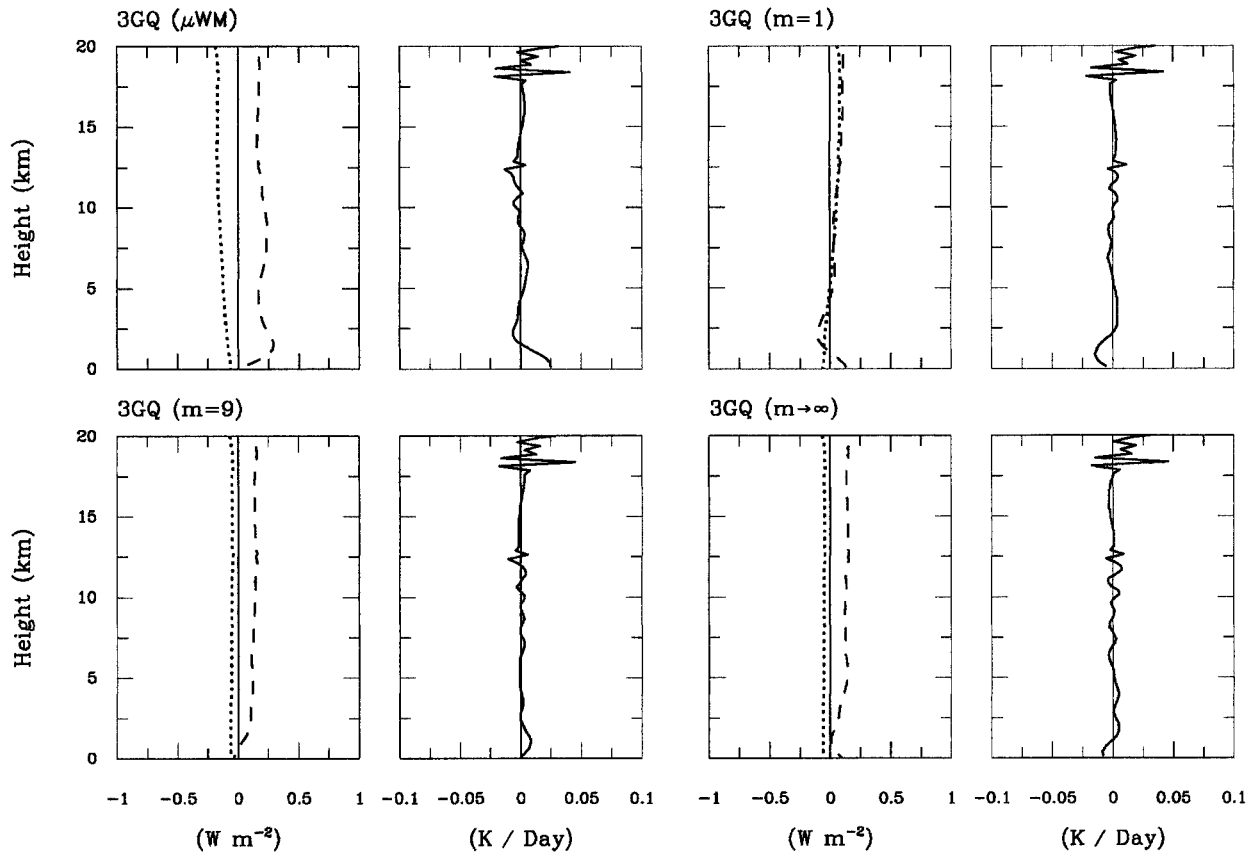


FIG. 4. The same as Fig. 2 but for 3GQ with different moment powers.

use the absorption approximation. The absorption approximation with scattering effect is systematically discussed in another work (Li and Fu 2000).

For 1GQ, it is found in Fig. 5 that the error in the cooling rate for the low cloud is over 2 K day^{-1} for the $1\text{GQ}(m \rightarrow \infty)$ (or the DF approximation). In GCMs, this large infrared cooling rate in the low cloud layers will lead to the convergence of water vapor more easily and will generate more clouds. This is a consistent problem for some GCMs. Figure 5 shows that the error incurred by the DF approximation is an important factor in accounting for the low cloud overcooling problem. For $1\text{GQ}(\mu\text{WM})$, the error in the cooling rate in the cloud layer is much smaller than that of the $1\text{GQ}(m \rightarrow \infty)$. However, such accuracy is accidental. From the flux profile for $1\text{GQ}(\mu\text{WM})$, the errors for fluxes in the cloud layer are larger than those of $1\text{GQ}(m \rightarrow \infty)$, especially for the downward flux. However, the errors for upward flux and downward flux are of the same sign, thereby canceling each other in calculating the cooling rate. Above the cloud layer the error in upward flux decreases rapidly. This is because the negative error for clear sky above the cloud layer compensates for the positive error in the upward flux above the cloud layer (see Fig. 2).

Flux analysis shows that the $1\text{GQ}(\mu\text{WM})$ is not superior to other Gaussian quadratures. The flux profiles help us to understand the errors in cooling rate. However, the flux profile is usually neglected in radiative transfer study, with only the values at the surface and the top of the atmosphere normally being shown.

In Fig. 5, we find that the errors decrease with the increase of the moment power like the clear-sky case. It is shown that the results of $1\text{GQ}(m \rightarrow \infty)$ are better than those of $1\text{GQ}(m = 1)$.

Figure 5 also shows the corresponding results of 2GQ. Compared with the results of 1GQ, the errors in the cloud layers are not as sensitive to the different Gaussian quadratures. This is because for 2GQ the difference in errors in the flux transmissions is small for different moments of Gaussian quadrature. Li and Fu (2000) clearly show that the errors are caused by the lack of scattering effect and they cannot be eliminated by increasing the accuracy of the flux transmittance. In the case of 2GQ, the error in upward fluxes for μWM does not decrease with height above the cloud layer like those in 1GQ, since in this case there is no longer the large negative error in the clear sky (see Fig. 3).

The results of the errors for the middle cloud case

Errors in Flux and Cooling Rate

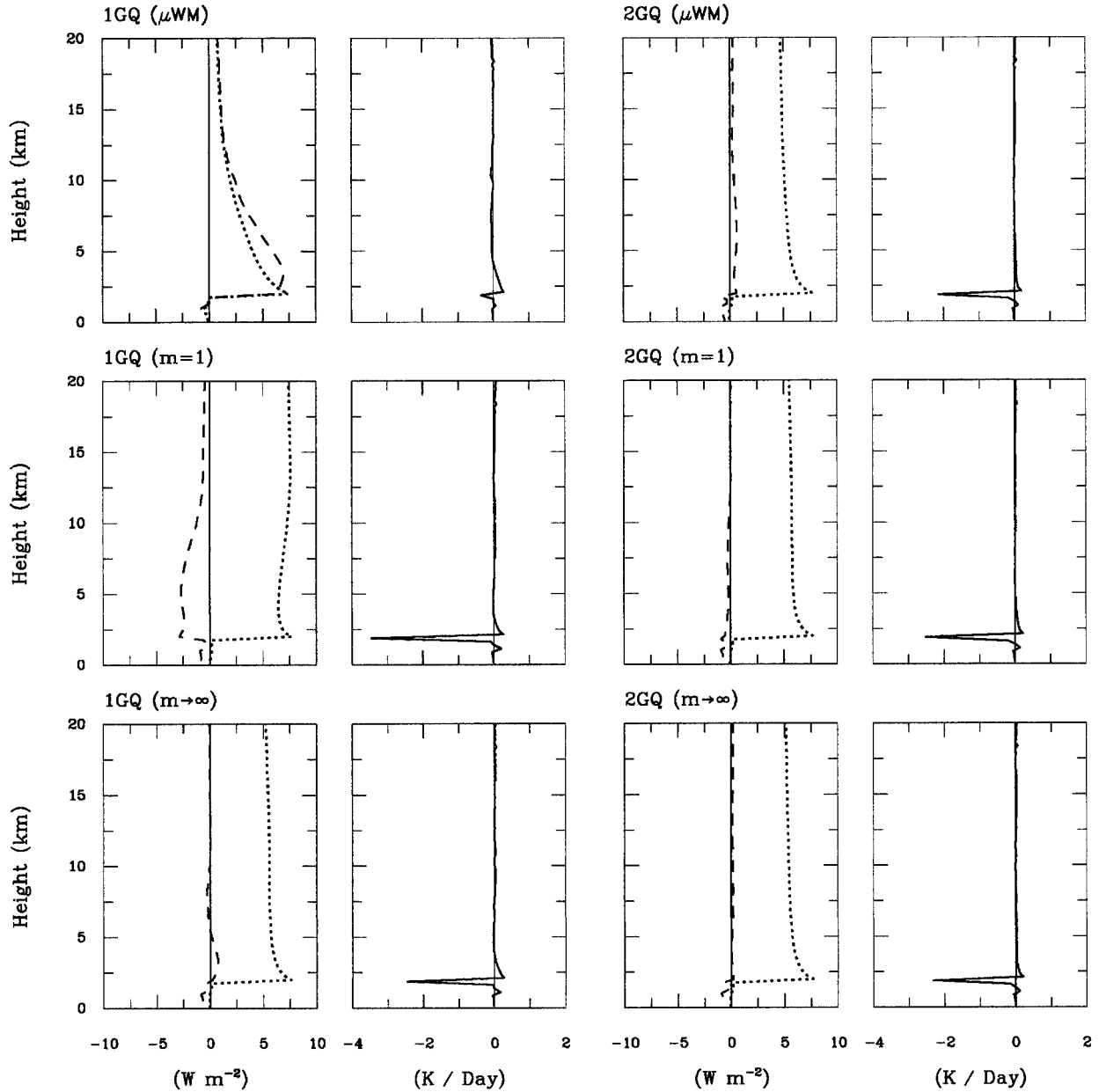


FIG. 5. Absolute errors for upward flux (dotted line), downward flux (dashed line), and cooling rate (solid line) for 1GQ and 2GQ with different moment powers, m . An overcast low cloud is positioned from 1.0 to 2.0 km with $LWC = 0.22 \text{ g m}^{-3}$ and $r_e = 5.98 \text{ } \mu\text{m}$.

are shown in Fig. 6. For 1GQ, the case of $m \rightarrow \infty$ is more accurate than that of μWM for both fluxes and cooling rates. Also, the accuracy increases with increasing moment power for the Gaussian quadrature. For 2GQ, the differences in fluxes and cooling rates are small, in the same manner as that of the low cloud case.

Figure 7 shows the results of the high cloud. Like the low cloud case, 1GQ(μWM) provides better results for fluxes and cooling rates. However, such accuracy is again accidental. Let us look at the upward flux. Large

negative error occurs below the cloud layer, which mostly cancels the positive errors inside the cloud [see the profiles of the upward flux for 1GQ($m = 1$) and 1GQ($m \rightarrow \infty$)]. For high cloud τ_{abs} is usually larger than 1. However, 1GQ(μWM) is valid for $\tau_{\text{abs}} < 0.3$. Beyond this region, the absolute error for the flux transmittance could be very large. Therefore, it is difficult to produce the accurate results in flux and cooling rate by 1GQ(μWM). If we consider the high cloud only without gaseous transmission, 1GQ(μWM) produces much large

Errors in Flux and Cooling Rate

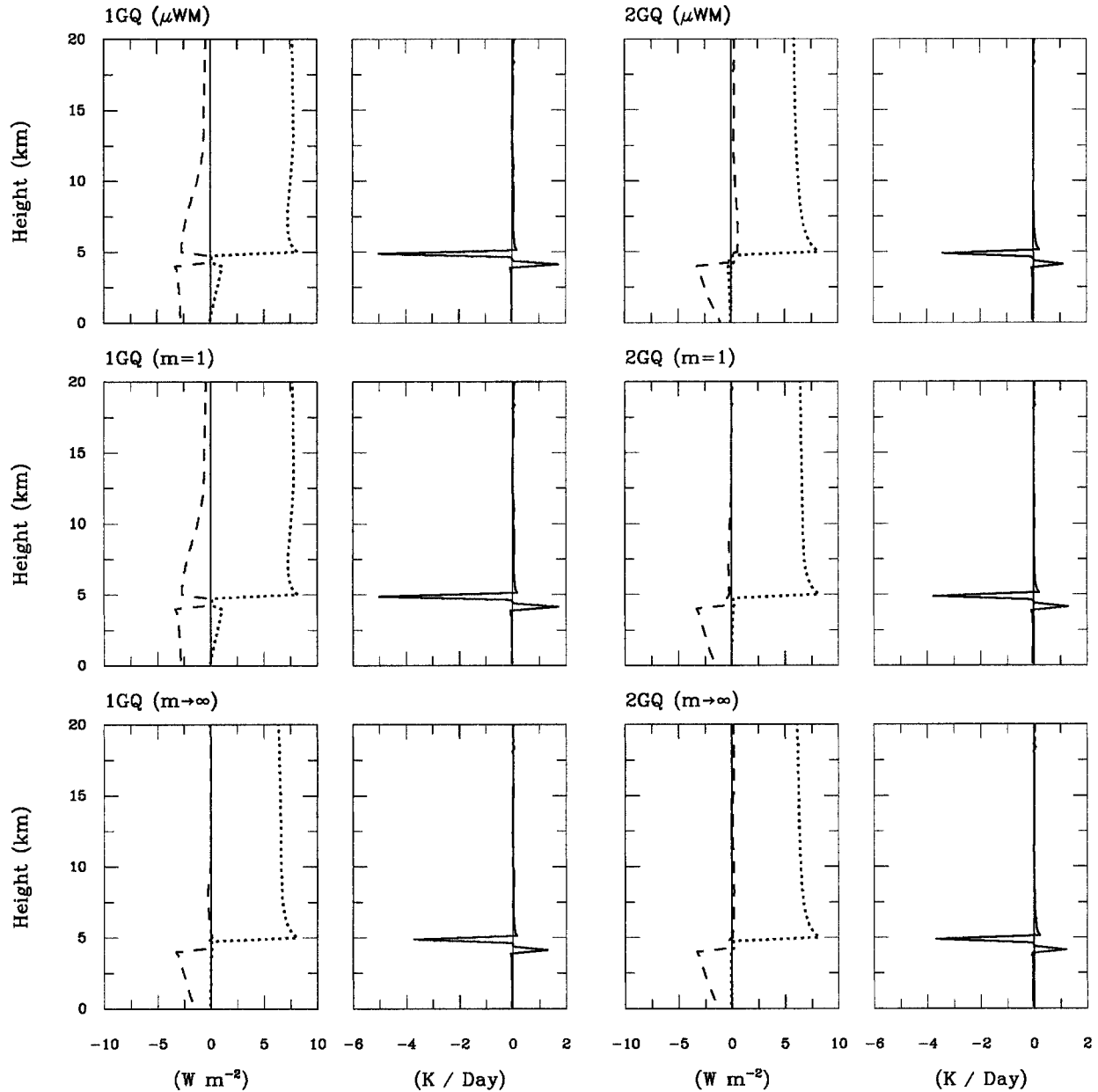


FIG. 6. The same as Fig. 5 but an overcast middle cloud is positioned from 4.0 to 5.0 km with $LWC = 0.28 \text{ g m}^{-3}$ and $r_e = 6.2 \text{ }\mu\text{m}$.

er errors in flux and cooling rate compared to those of $1GQ(m \rightarrow \infty)$.

Unlike the cases of low cloud and middle cloud, 2GQ generally produces much better results in fluxes and cooling rates. This is because 2GQ (equivalent to a four-stream scheme) can more properly handle the highly anisotropic radiation inside the high clouds (Li and Fu 2000). Besides, the optical depth for a high cloud is smaller than that of low or middle clouds mostly with a magnitude of 1–5. Figure 1 shows that 2GQ generally

produces much better results in the flux transmittance for τ_{abs} in the range 1–3, as compared with 1GQ.

4. Discussion and conclusions

The flux transmittance can be directly evaluated using Gaussian integration by μWM or Gaussian integration of moment power $m = 1$. For 1GQ, the corresponding diffusivity factor $1/\bar{\mu}_1$ would be 2 or 1.5. However, for historical reasons, neither of these two values are used.

Errors in Flux and Cooling Rate

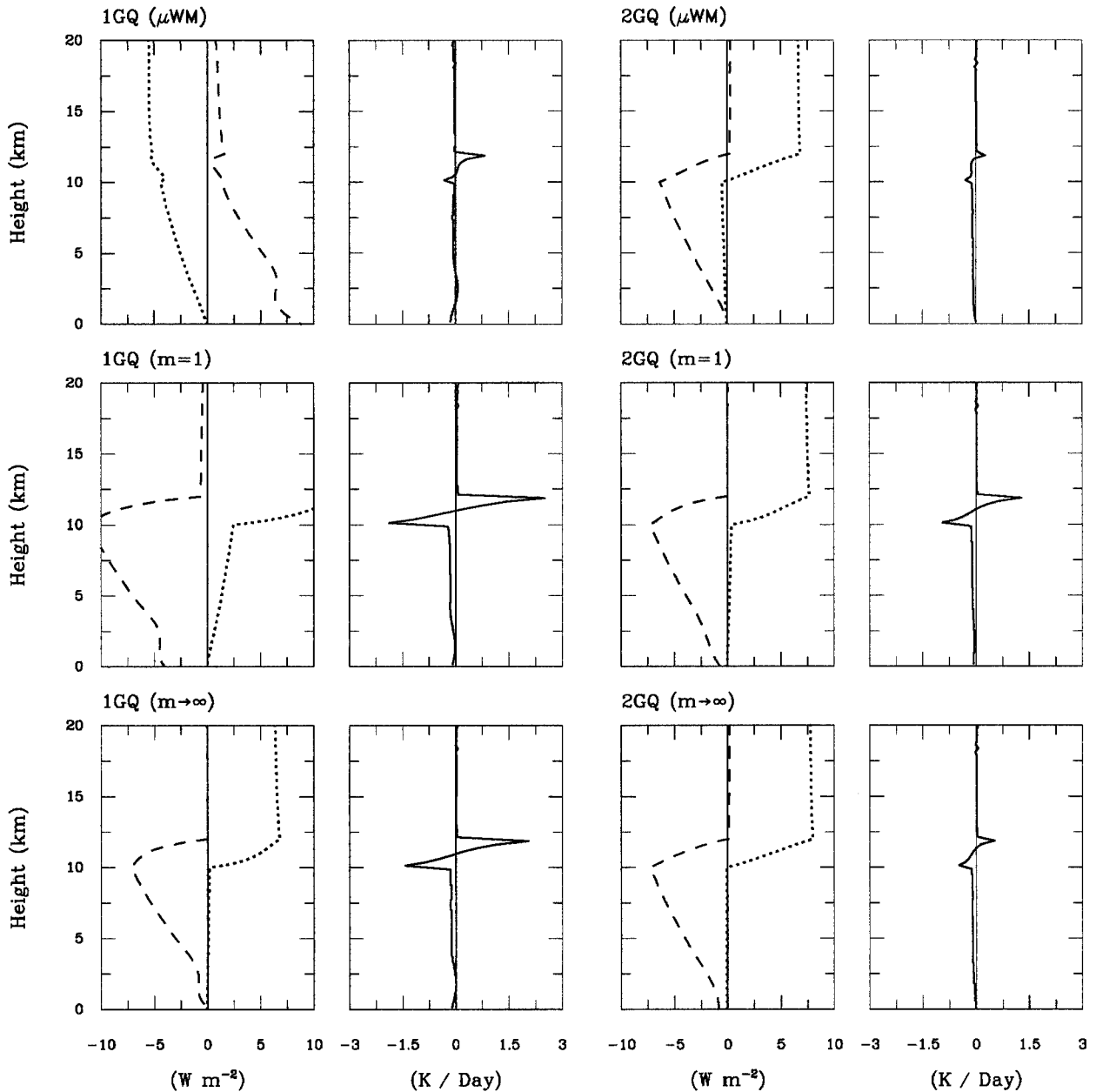


FIG. 7. The same as Fig. 5 but an overcast high cloud is positioned from 10 to 12 km, with IWC = 0.0048 g m⁻³ and $D_e = 41.5 \mu\text{m}$.

Instead the diffusivity factor $1/\bar{\mu}_1 = 1.66$ proposed by Elsasser (1942) is widely used. In this work we have shown that the Gaussian quadrature with higher-moment power ($m > 1$) can also be used to evaluate the flux transmittance. For Gaussian quadrature of a higher-moment power, the accuracy in the thin τ_{abs} region is generally improved compared to that of a lower-moment power. For the limit of $m \rightarrow \infty$ we obtained $1/\bar{\mu}_1 = e^{1/2} = 1.648\,721\,3$ in 1GQ. Though $e^{1/2}$ and 1.66 are very close, using $e^{1/2}$ has a more solid mathematical basis.

Also, 1GQ($m \rightarrow \infty$) has its higher-order extension $n\text{GQ}(m \rightarrow \infty)$ ($n = 2, 3, \dots$). It is shown that 1GQ($m \rightarrow \infty$) is an adequate choice. For $\tau_{\text{abs}} < 1$, 1GQ($m \rightarrow \infty$) is valid (relative error of the flux transmittance less than 10%). However, beyond this region, the absolute value of the flux transmittance is very small.

In a one-dimensional radiative transfer model, the diffusivity factor $1/\bar{\mu}_1 = 1.648\,721\,3$ generally produces more accurate results than those by directly using Gaussian quadrature [i.e., 1GQ(μWM) and 1GQ($m =$

1)] and other values of moment power for 1GQ. Recently, Li and Fu (2000) showed that the cloud infrared scattering can be considered in the absorption approximation through a perturbation method. In this case, LF99 find that $1/\bar{\mu}_1 = e^{1/2}$ always produces a better result in comparison with that of $1/\bar{\mu}_1 = 1.66$.

More accurate results can be achieved through higher-node Gaussian quadratures, such as 2GQ or 3GQ. Generally, an n -node Gaussian quadrature corresponds to a $2n$ -stream radiative transfer scheme. The calculations show that in the case of higher-node Gaussian quadrature, the limit of $m \rightarrow \infty$ always gives the better results compared to other moments.

The flux transmittance in the DF approximation has the same mathematical expression as the radiance transmittance. The exponential function means that the transmittance of two layers is simply the product of each individual layer's transmittance, a property that ensures computational efficiency. The computational advantage of the DF approximation or 1GQ is kept in the higher-node Gaussian quadratures. Therefore, the higher-node Gaussian quadrature methods can be implemented in an infrared radiation model directly, no matter whether the (correlated) k distribution or band model is used.

The results of Gaussian quadrature with different moment powers in Eqs. (A4)–(A6) and the limit case of moment power approaching infinity are general. It can be applied to any integral with limit of 0 to 1. The so-called double Gaussian quadrature used in discrete ordinate method for solar radiation is just the case of μ WM by directly applying Gaussian quadrature with the zero moment (Stamnes et al. 1989; Fu and Liou 1993). In principle, the higher moments and the limit of the moment power approaching infinity in the Gaussian quadrature can be applied to scattering cases for both infrared and solar radiation. This is a topic that needs further exploration.

In the one-dimensional infrared radiation code we used, 2GQ costs about 10% more CPU time compared to the DF approximation, and the increase of CPU time is approximately proportional to the increase of the node of Gaussian quadrature. Therefore, computing time is affordable when using a two-node Gaussian quadrature (four-stream scheme for absorption approximation) in a GCM.

Acknowledgments. The author would like to thank Drs. M.-D. Chou, M. Holzer, and N. McFarlane, Mr. T. H. Lindner, and the two anonymous reviewers for their help.

APPENDIX A

Gaussian Integration of Moments

By n -node Gaussian quadrature, the integration of moment l is evaluated by

$$\int_0^1 x^l f(x) dx \approx \sum_{i=1}^n b_i f(x_i) \quad (l = 0, 1, 2, \dots), \quad (\text{A1})$$

where x_i is the abscissa and b_i is the weight. Following Abramowitz and Stegun (1964) [for the detailed theoretical discussion see Krylov (1962)], x_i is i th root of

$$q_n(x) = 0, \quad (\text{A2})$$

where

$$q_n(x) = \sqrt{l + 2n + 1} P_n^{(l,0)}(1 - 2x),$$

$P_n^{(\alpha,\beta)}$ (x) is the Jacobi polynomial,

$$P_n^{(\alpha,\beta)}(x) = \frac{1}{2^n} \sum_{i=0}^n \binom{n+\alpha}{i} \binom{n+\beta}{n-i} (x-1)^{n-i} (x+1)^i.$$

The weight is given by

$$b_j = 1 / \sum_{i=0}^{n-1} [q_i(x_j)]^2. \quad (\text{A3})$$

For the integral of the flux transmittance in Eq. (4) we can directly apply Eq. (A1) for either $l = 0$ or $l = 1$ as shown in Eqs. (8)–(9). Also, we can use a higher-moment power Gaussian quadrature to evaluate the integral like Eq. (3). By a substitution, $\mu = x^{(m+1)/2}$, we have

$$\begin{aligned} 2 \int_0^1 f(\mu) \mu d\mu &= (m+1) \int_0^1 x^m f(x^{(m+1)/2}) dx \\ &\approx \sum_{i=1}^n w_i f(\bar{\mu}_i), \end{aligned} \quad (\text{A4})$$

where

$$1/\bar{\mu}_i = 1/x_i^{(m+1)/2}, \quad \text{and} \quad (\text{A5})$$

$$w_i = (m+1)b_i. \quad (\text{A6})$$

The values of x_i and b_i are listed in Table 1. The values for $m = 0, 1, 3, 5$ are from Abramowitz and Stegun (1964), and $m = 7$ and 9 are calculated by the author. Note that the values of x_i and b_i for $m = 0$ in Table 1 are the same as those for Eq. (A1) as $l = 0$. However, the results are different (see Fig. 1).

For the limit of $m \rightarrow \infty$, based on Eqs. (A4)–(A6), through lengthy algebraic calculation we obtain for $n = 1$,

$$1/\bar{\mu}_1 = e^{1/2} = 1.6487213, \quad (\text{A7})$$

$$w_1 = 1; \quad (\text{A8})$$

for $n = 2$,

$$1/\bar{\mu}_{1,2} = e^{1 \pm (1/\sqrt{2})} = 1.3402997, 5.5129882, \quad (\text{A9})$$

$$w_{1,2} = \frac{1}{4 \pm 2\sqrt{2}} = 0.8535534, 0.1464466; \quad (\text{A10})$$

for $n = 3$,

$$1/\bar{\mu}_{1,2,3} = e^{(1/2)\psi_{1,2,3}}, \quad (\text{A11})$$

$$w_{1,2,3} = \frac{1}{3 - 6\psi_{1,2,3} + 6\psi_{1,2,3}^2 - 2\psi_{1,2,3}^3 + 0.25\psi_{1,2,3}^4}, \quad (\text{A12})$$

where $\psi_{1,2,3} = 3 - 3\sqrt{3} \cos\theta_{1,2,3}$, with $\theta_1 = \frac{1}{3} \arccos(-1/\sqrt{3})$, $\theta_2 = \frac{1}{3} \arccos(-1/\sqrt{3} + 120^\circ)$, and $\theta_3 = \frac{1}{3} \arccos(-1/\sqrt{3} + 240^\circ)$. We eventually get

$$1/\bar{\mu}_{1,2,3} = 1.2310744, 23.2190344, \quad (\text{A13})$$

$$3.1491749;$$

$$w_{1,2,3} = 0.7110930, 0.0103893,$$

$$0.2785176. \quad (\text{A14})$$

In the following, we will examine the characteristics of the errors for the limit of $m \rightarrow \infty$, from the remainder point of view. For the flux transmittance $f(\mu) = \exp(-\tau_{\text{abs}}/\bar{\mu})$, we have (Krylov 1962)

$$(m+1) \int_0^1 x^m \exp(-\tau_{\text{abs}}/x^{(m+1)/2}) dx \\ = \sum_{i=1}^n w_i \exp(-\tau_{\text{abs}}/\bar{\mu}_i) + R_n; \quad (\text{A15})$$

the remainder is

$$R_n = (m+1) \frac{f^{(2n)}(\xi)}{(m+2n+1)(2n)!} \left[\frac{n!(m+n)!}{(m+2n)!} \right]^2, \quad (\text{A16})$$

where $(2n)$ in $f^{(2n)}(\xi)$ means $2n$ derivatives, and $0 < \xi < 1$ depending on m , n , and τ_{abs} . For $n = 1$ we have

$$R_1 = \frac{1}{2(m+2)^2} \frac{(m+1)}{(m+3)} f^{(2)}(\xi), \quad (\text{A17})$$

where

$$f^{(2)}(\xi) = \frac{1}{4} [(m+3)^2 \xi^{-(m+3)} \tau_{\text{abs}}^2 \\ - (m+1)(m+3) \xi^{-(m+5)/2} \tau_{\text{abs}}] \\ \times \exp(-\tau_{\text{abs}} \xi^{-(m+1)/2}).$$

For a large m , ξ can be expanded as $\xi = a_0 + a_1/m + a_2/m^2 + \dots$, where a_i are the expansion coefficients, depending on the node n and τ_{abs} . Obviously the positive power terms are not allowed to exist in the expansion. The restriction of $0 < \xi < 1$ for $m \rightarrow \infty$ requires $a_0 \leq 1$. It is easy to show that for $a_0 < 1$,

$$\lim_{m \rightarrow \infty} R_1 \equiv 0.$$

This is incorrect since the remainder cannot be zero. If $a_0 = 1$, a_1 in the leading term has to be negative. We derive

$$\lim_{m \rightarrow \infty} R_1 = \frac{c\tau_{\text{abs}}}{8} (c\tau_{\text{abs}} - 1) e^{-c\tau_{\text{abs}}}, \quad (\text{A18})$$

where $c = e^{-(1/2)a_1}$. Similarly, we obtain

$$\lim_{m \rightarrow \infty} R_2 = \frac{c\tau_{\text{abs}}}{96} (c^2\tau_{\text{abs}}^3 - 6c^2\tau_{\text{abs}}^2 + 7c\tau_{\text{abs}} - 1) \\ \times e^{-c\tau_{\text{abs}}}, \quad (\text{A19})$$

$$\lim_{m \rightarrow \infty} R_3 = \frac{c\tau_{\text{abs}}}{1280} (c^5\tau_{\text{abs}}^5 - 15c^4\tau_{\text{abs}}^4 + 65c^3\tau_{\text{abs}}^3 \\ - 90c^2\tau_{\text{abs}}^2 + 31c\tau_{\text{abs}} - 1) e^{-c\tau_{\text{abs}}}. \quad (\text{A20})$$

The remainders are approximately proportional to $1/10^n$, which tells why errors dramatically decrease with the increase of node n . The remainders always approach zero as τ_{abs} decreases, which tells us why errors are extremely small in the very thin τ_{abs} regions. Moreover, from Eqs. (A18)–(A20), it is found that there could exist one point in τ_{abs} with $R_1(m \rightarrow \infty) = 0$, three points in τ_{abs} with $R_2(m \rightarrow \infty) = 0$, and five points in τ_{abs} with $R_3(m \rightarrow \infty) = 0$. These results are confirmed in Fig. 1. For a finite m , R_2 and R_3 are extremely complicated. The relations for the error are therefore difficult to explore.

APPENDIX B

Solutions of Radiative Transfer Equation for the Infrared

The solution of Eq. (2) can be equivalently written as

$$F_i^\uparrow = \pi \sum_{k=i}^{N-1} B_{k+(1/2)} (T_{i,k+1} - T_{i,k}) + B_s T_{i,N}, \quad (\text{B1a})$$

and

$$F_i^\downarrow = \pi \sum_{l=1}^{i-1} B_{l+(1/2)} (T_{li} - T_{l+1,i}), \quad (\text{B1b})$$

where F_i^\uparrow (F_i^\downarrow) is the upward (downward) flux at level i , $T_{k,l}$ is the transmittance between two levels k and l , $B_{i+(1/2)}$ is the Planck function for layer i (between level i and level $i+1$), level 1 is the top of the atmosphere, and level N is the surface.

If we focus on one single layer, the solution of Eq. (1) is

$$I_i^\uparrow(\mu) = I_{i+1}^\uparrow(\mu) \exp(-\tau_{\text{abs}i}/\mu) \\ + B_{i+(1/2)} [1 - \exp(-\tau_{\text{abs}i}/\mu)] \quad \text{and} \quad (\text{B2a})$$

$$I_i^\downarrow(-\mu) = I_{i-1}^\downarrow(-\mu) \exp(-\tau_{\text{abs}i-1}/\mu) \\ + B_{i-(1/2)} [1 - \exp(-\tau_{\text{abs}i-1}/\mu)], \quad (\text{B2b})$$

where $I_i^\uparrow(\mu)$ [$I_i^\downarrow(-\mu)$] is the upward (downward) intensity at level i , $\tau_{\text{abs}i} = (1 - \omega_i)\tau_i$, and ω_i and τ_i are the single scattering albedo and optical depth for layer i , respectively. The physical meaning of Eq. (B2) is very clear. The first term represents the contribution to intensity from lower (upper) boundary with exponential decay by absorption. The second term represents contribution to intensity from the thermal emission inside

the layer. Fu et al. (1997) have considered the non-isothermal layer case and obtained a more general solution.

The fluxes of intensities in Eq. (B2) are

$$F_i^\uparrow = 2\pi \int_0^1 I_i^\uparrow(\mu)\mu d\mu \quad \text{and} \quad (\text{B3a})$$

$$F_i^\downarrow = 2\pi \int_0^1 I_i^\downarrow(-\mu)\mu d\mu, \quad (\text{B3b})$$

which can be obtained through Gaussian quadrature of Eq. (A1) or Eq. (A4). Unlike the solution of Eq. (B1), the Gaussian quadrature does not directly apply to the flux transmittance of Eq. (4). It applies to the intensities in Eq. (B2). However, in Eq. (B2) or a more general solution in Fu et al. (1997), the radiance transmittance $\exp(-\tau_{\text{abs}}/\mu)$ is the dominate factor.

Solutions (B1) and (B2) are equivalent in mathematics. In solution (B1) the upward (downward) flux at one level is determined by the thermal emission and absorption from all the layers below (above) that level. Therefore, the computing time is quadratically proportional to the model layer. In contrast from Eq. (B1), in Eq. (B2) all the exchange contributions from outside of this layer are represented by the boundary conditions. Therefore, the computing time is linearly proportional

to the model layer. Regardless, the band model method or correlated-k method is used to calculate the gaseous transmission.

REFERENCES

- Abramowitz, M., and I. A. Stegun, 1964: *Handbook of Mathematical Functions with Formulas, Graphs, and Mathematical Tables*. Applied Mathematics Series, Vol. 55, National Bureau of Standards, 1045 pp.
- Chou, M. D., and M. J. Suarez, 1994: An efficient thermal infrared radiation parameterization for use in general circulation models. NASA Tech. Memo. 104606, Vol. 3.
- Elsasser, W. M., 1942: *Heat Transfer by Infrared Radiation in the Atmosphere*. Harvard Meteorological Studies, Vol. 6, Harvard University Press, 107 pp.
- Fu, Q., and K. N. Liou, 1993: Parameterization of the radiative properties of cirrus clouds. *J. Atmos. Sci.*, **50**, 2008–2025.
- , —, M. C. Cribb, T. P. Charlock, and A. Grossman, 1997: On multiple scattering in thermal infrared radiative transfer. *J. Atmos. Sci.*, **54**, 2799–2812.
- Krylov, V. I., 1962: *Approximate Calculation of Integrals*. Macmillan, 357 pp.
- Li, J., and Q. Fu, 2000: Absorption approximation with scattering effect for infrared radiation. *J. Atmos. Sci.*, in press.
- Stamnes, K., S. C. Tsay, W. Wiscombe, and K. Jayaweera, 1988: A numerically stable algorithm for discrete-ordinate-method radiative transfer in multiple scattering and emitting layered media. *Appl. Opt.*, **27**, 2502–2509.
- Toon, O. B., C. P. McKay, and T. P. Ackerman, 1989: Rapid calculation of radiative heating rates and photodissociation rates in inhomogeneous multiple scattering atmospheres. *J. Geophys. Res.*, **94**, 16 287–16 301.